Strengthening and recovery in AX41 magnesium alloy reinforced with short Saffil fibres

Z. Trojanová*, P. Lukáč, Z. Száraz

Department of Physics of Materials, Faculty of Mathematics and Physics, Charles University, Ke Karlovu 5, CZ-121 16 Prague 2, Czech Republic

Received 22 October 2007, received in revised form 30 October 2007, accepted 5 November 2007

Abstract

AX41 magnesium alloy (4Al-1Ca-balance Mg in wt.%) reinforced with short α-Al_2O_3 fibres (Saffil®) has been deformed in compression at temperatures between 23 and 300 °C. The yield stress and the maximum stress decrease with increasing testing temperature. The influence of reinforcement on both characteristic stresses falls down with increasing temperature. Possible hardening and softening mechanisms are discussed. Stress relaxation tests were performed in order to reveal features of the thermally activated dislocation motion. Internal and effective components of the applied stress have been estimated. The apparent activation volume decreases with increasing effective stress. The values of the activation volume as well as the activation enthalpy indicate that the main thermally activated process is connected with the rapid decrease of the internal stress with deformation temperature.

K e y w o r d s: magnesium alloy based composite, compression deformation, stress relaxation test, thermally activated processes

1. Introduction

Interest in an increase of the strength (and creep resistance) of lightweight metallic materials has grown significantly over the last decade. Magnesium, aluminium and titanium alloys are very attractive for various structural applications. The influences of different processing techniques, composition, heat treatment and grain size on the mechanical properties and deformation behaviour have been investigated [1–9]. Investigations have extended beyond these alloys to an interesting group of TiAl-based intermetallic alloys, e.g. [10–13] and composites with Mg alloys matrix [14–17], Al alloys matrix [18, 19] and alloys reinforced with nanoparticles [20]. In recent years metal matrix composites (MMCs) have attracted worldwide attention as a result of their potential to replace their monolithic counterparts primarily in automotive, aerospace and energy generation sectors. Adding the reinforcement to the matrix has advantages and also disadvantages. Among advantages an increase of elastic modulus E, the yield stress as well as the strength, creep resistance, damping and wear resistance, and a decrease of the thermal expansion coefficient are the most important. On the other hand, composites exhibit low ductility and they are produced by more complicated and expensive techniques.

It is generally accepted that during deformation of a composite, deformation process occurs in the matrix and short ceramic fibres deform only elastically. An increase in the flow stress in the composite is caused mainly by the following four reasons:

– Load transfer from the matrix to fibres;

– Direct impact of fibres as impenetrable obstacles for the dislocation motion;

– Influence of fibres on the development of the dislocation substructure in the matrix;

– Influence of fibres on the microstructure formation.

While the intrinsic mechanical and physical properties of the reinforcement (stiffness, strength and thermal expansion) are dictated by its chemical nature, the geometric and topological parameters of the reinforcement (shape, size, volume fraction, spatial orientation, and distribution) can be altered during processing.

*Corresponding author: tel.: +420 221911357; fax: +420 221911490; e-mail address: ztrojan@met.mff.cuni.cz

The applied stress σ necessary for deformation of any polycrystalline material can be divided into two components: the internal (athermal) stress σ_i and the effective stress σ^*, i.e. one can write:

$$\sigma = \sigma_\mathrm{i} + \sigma^*. \tag{1}$$

In a composite the athermal component includes the stress, which is necessary for deformation due to the load transfer σ_LT, and $\sigma_\mathrm{i}^\mathrm{D}$ the stress necessary for generation of dislocations, their movement and storage. The flow stress σ_LT necessary for composite deformation due to the load transfer can be calculated as [21]:

$$\sigma_\mathrm{LT} = \sigma_\mathrm{m}\left[1 + \frac{(L + d_\mathrm{t})\,A}{4L}\right] f + \sigma_\mathrm{m}\,(1 - f)\,, \tag{2}$$

where σ_m is the yield stress in the matrix, f is the volume fraction of fibres, L is the fibre size in the direction of the applied stress, d_t is the fibre size in the perpendicular direction and A is the fibre aspect ratio (L/d_t). The model is based on the simplifying assumption of uniform matrix deformation and therefore, it yields a very simplified expression for stiffness and strength contribution. The internal stress $\sigma_\mathrm{i}^\mathrm{D}$ resulting from long-range internal stresses impeding the plastic flow is done as:

$$\sigma_\mathrm{i}^\mathrm{D} = \alpha_1 G b \rho_\mathrm{t}^{1/2}, \tag{3}$$

where G is the shear modulus, α_1 is a constant describing interaction between dislocations, b is the Burgers vector of dislocations and ρ_t is the total dislocation density. The effective shear stress σ^* acts on dislocations during their thermally activated motion when they overcome short range obstacles. The mean velocity of dislocations v is connected with the plastic strain rate by the Orowan equation:

$$\dot{\varepsilon} = (1/\psi)\,\rho_\mathrm{m}\,b\,v, \tag{4}$$

where ρ_m is the density of mobile dislocations and ψ is Taylor orientation factor. The most common equation used in describing the average dislocation velocity as a function of the effective stress is an Arrhenius type. The plastic strain rate $\dot{\varepsilon}$ for a single thermally activated process can be expressed as:

$$\dot{\varepsilon} = \dot{\varepsilon}_0 \exp\left[-\Delta G\left(\sigma^*\right)/kT\right], \tag{5}$$

where $\dot{\varepsilon}_0$ is a pre-exponential factor containing the mobile dislocation density, the average area covered by the dislocations in every activation act, the Burgers vector, the vibration frequency of the dislocation line, and the geometric factor. T is the absolute temperature and k is the Boltzmann constant. $\Delta G(\sigma^*)$ is the change in the Gibbs free enthalpy depending on the effective stress $\sigma^* = \sigma - \sigma_\mathrm{i}$ and the simplest form is

$$\Delta G(\sigma^*) = \Delta G_0 - V\sigma^* = \Delta G_0 - V(\sigma - \sigma_\mathrm{i}). \tag{6}$$

Here ΔG_0 is the Gibbs free enthalpy necessary for overcoming a short range obstacle without the stress and $V = bdL_\mathrm{c}$ is the activation volume, where d is the obstacle width and L_c is the mean length of dislocation segments between obstacles.

The stress relaxation technique is very useful method to study the thermally activated processes and to reveal the dominant process occurring during plastic deformation. In a stress relaxation (SR) test, the specimen is deformed to a certain stress σ_0 and then the machine is stopped and the stress is allowed to relax. The stress decreases with the time t. The specimen can be again reloaded to a higher stress (load) and the SR test may be repeated. The time derivative $\dot{\sigma} = \mathrm{d}\sigma/\mathrm{d}t$ is the stress relaxation rate and $\sigma = \sigma(t)$ is the flow stress at time t during the SR. The stress relaxation tests are very often analysed under the assumption that the SR rate is proportional to the strain rate $\dot{\varepsilon}$, according to [22], as:

$$\dot{\varepsilon} = -\dot{\sigma}/M, \tag{7}$$

where M is the combined modulus of the specimen – machine set. The stress decrease with the time during the SR can be described by the well known Feltham equation [23]:

$$\Delta\sigma(t) = \sigma(0) - \sigma(t) = \alpha \ln(\beta t + 1), \tag{8}$$

where $\sigma(0) \equiv \sigma_0$ is the stress at the beginning of the stress relaxation at time $t = 0$, β is a constant,

$$\alpha = \frac{kT}{V}. \tag{9}$$

The aim of this work is to study strengthening and thermally activated processes occurring during plastic deformation of an AX41 magnesium alloy reinforced with short ceramic fibres.

2. Experimental procedure

Commercial AX41 alloy (Mg-4wt.%Al-1wt.%Ca) was used as the matrix alloy. The alloy was reinforced with δ-Al_2O_3 short fibres (Saffil®) with a mean diameter of 3 μm and a mean length about 87 μm (measured after squeeze casting). The preform consisting of Al_2O_3 short fibres showing a planar isotropic fibre distribution and a binder system (containing Al_2O_3 and starch) was preheated to a temperature higher than

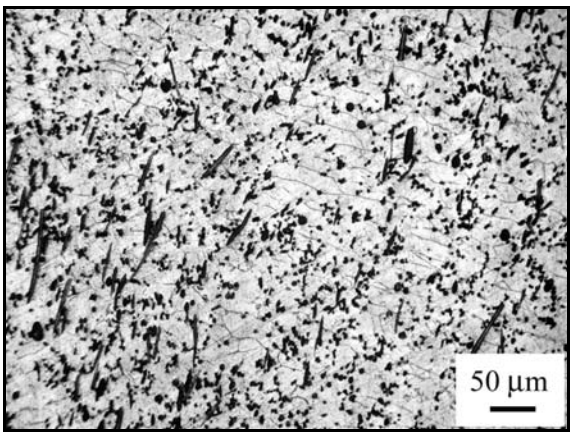

Fig. 1. Microstructure of the undeformed sample; the surface plane perpendicular to the stress axis.

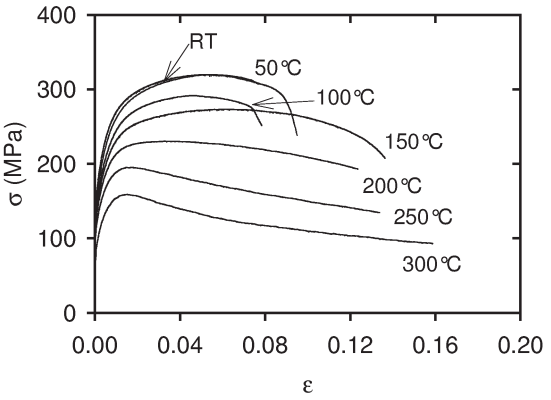

Fig. 2. Stress-strain curves obtained at various temperatures.

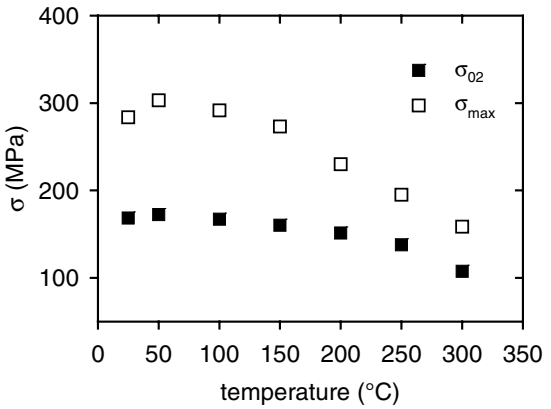

Fig. 3. Temperature dependences of the yield stress and the maximum stress.

the melt temperature of the alloy and then inserted into a preheated die (290 to 360 °C). The two-stage application of the pressure resulted in the metal matrix composite with a fibre volume fraction of 13 vol.% of fibres.

Samples for compression tests, machined from a composite block, had a square cross-section of 5 mm × 5 mm and a length of 10 mm. Samples were deformed in an Instron 1186 testing machine at a constant crosshead speed giving an initial strain rate of 8.3×10^{-5} s^{-1} over the temperature range from room temperature up to 300 °C. The temperature in the furnace was kept with an accuracy of ±1 °C. Sequential stress relaxation tests were performed at increasing stress along a stress-strain curve. Duration of the SR was 300 s. Ductility of the alloy at room temperature is very low and therefore the SR tests were performed at elevated temperatures. On the other hand, recovery during the SR test was observed at 300 °C and hence, the results obtained at this temperature were not taken into account because the above given equations describing the SR were derived under an assumption that the internal stress σ_i is constant during the SR. Only in the first SR test at 300 °C, recovery may be considered to be negligible, i.e. σ_i is constant.

Components of the applied stress (σ_i, σ^*) were estimated using Li's method [24, 25]. The SR curves were fitted to the power law function in the form: $\sigma - \sigma_i = [a\,(m-1)]^{\frac{1}{1-m}}\,(t+t_0)^{\frac{1}{1-m}}$, where a, t_0 and m are fitting parameters. Sections of composite castings were polished and the microstructure was examined using the Olympus light microscope.

3. Experimental results

A typical feature of the AX41 alloy consists from solid solution of Al in Mg, α-Mg grains decorated by particles. SEM showed $Mg_{17}Al_{12}$ intermetallic phase surrounded with smaller particles of Al_2Ca. The microstructure of the composite is more complicated as it can be seen in Fig. 1; the micrograph was taken from the section perpendicular to the fibre planes. It is obvious that the planar random distribution of fibres is not perfect. The stress-strain curves obtained at various temperatures are introduced in Fig. 2. The temperature dependence of the yield stress as well as the maximum stress is given in Fig. 3. While the yield stress slowly decreases with temperature up to 200 °C, the decrease at higher temperatures is stronger. The maximum stress decreases with increasing temperature at temperatures higher than 50 °C. The differences between the yield stress and the maximum stress indicate that some work hardening exists at all the temperatures studied. An example of the stress relaxation curve obtained at 200 °C is shown in Fig. 4. The applied stress σ decreases during the stress relaxation test. When the internal dislocation stress and mobile dislocation density are constant the stress decrease is due to a decrease of the effective stress σ^*. In the

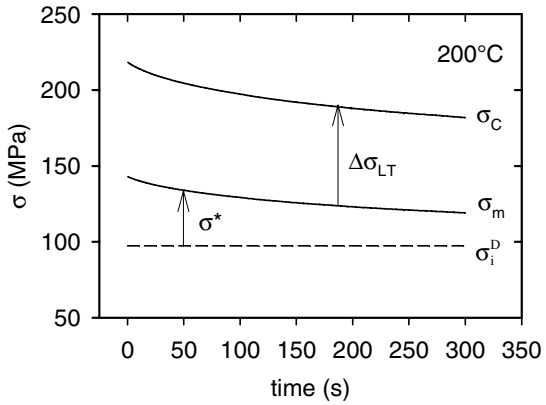

Fig. 4. Stress relaxation curve measured at 200 °C. Components of the applied stress are indicated.

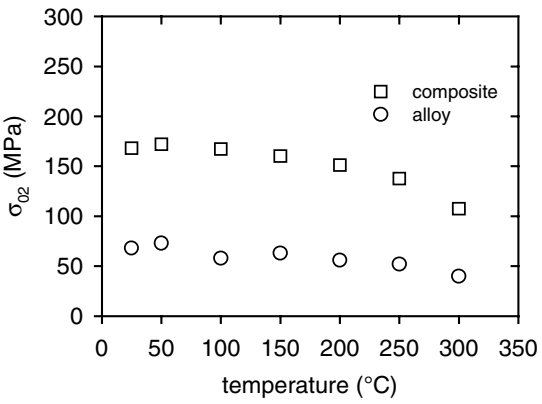

Fig. 5. Comparison of the temperature dependence of the yield stress measured for composite and monolithic alloy.

composite sample, the decrease of the effective stress in the matrix causes a decrease in the load transfer component. It is demonstrated in Fig. 4, where stress component due to load transfer σ_{LT} has been calculated using relationship (2).

4. Discussion

4.1. Fibre strengthening

Reinforcing impact of Saffil short fibres on the yield stress at various temperatures is introduced in Fig. 5. It can be seen that the strengthening effect of fibres at the very beginning of plastic deformation at room temperature exhibits about 100 MPa and decreases with increasing temperature to about 70 MPa at 300 °C. The influence of the reinforcing fibres on the maximum stress is weaker in comparison with the yield stress, it exhibits at room temperature about 90 MPa and at 300 °C only 25 MPa.

Trojanová et al. [26] analysed various strengthening mechanisms in Mg alloys reinforced by short Saffil fibres. The most significant contributions were found to be the load transfer from the matrix to the fibres and the influence of the increased dislocation density arising from internal thermal stresses. Other possible mechanisms do not influence any level of deformation stresses by a significant manner. In the literature several theoretical models were developed to explain the strengthening in composites [27–30]. As it follows from Eq. (1), the load transfer is more effective for higher values of the fibre aspect ratio A, i.e. longer fibres; however, on the other hand, the anisotropy of such a composite is higher.

The internal stress increases due to dislocation storage in the matrix, $\sigma_{\mathrm{i}}^{\mathrm{D}} \propto \rho_{\mathrm{t}}^{1/2}$, because the total dislocation density ρ_{t} increases due to two reasons: (a) generation of thermal dislocations and (b) the presence of dislocations geometrically necessary. Typically, the coefficient of thermal expansion (CTE) of the matrix is higher than CTE of a ceramic reinforcement. When the metal matrix composite is cooled from a higher temperature to room temperature, misfit strains occur because of different thermal contractions at the matrix-reinforcement interface. These strains induce thermal stresses that may be higher than the yield stress of the matrix. The thermal stresses may be sufficient to generate new dislocations at the interfaces between the matrix and the reinforcements. Therefore, after cooling a composite, the dislocation density in the matrix increases. The density of newly formed dislocation, near reinforcement fibres or particles can be calculated as [27]:

$$\rho_{\mathrm{T}} = \frac{Bf\Delta\alpha\,\Delta T}{b\,(1-f)}\,\frac{1}{t_{\mathrm{m}}}, \tag{10}$$

where t_{m} is a minimum size of the reinforcing phase particles or fibres, b is the magnitude of the Burgers vector of the newly created dislocations, B is a geometrical constant ($B = 10$ for fibres and $B = 12$ for particles), $\Delta\alpha\Delta T$ is the thermal strain ($\Delta\alpha$ is the difference in the coefficients of thermal expansion and ΔT is the temperature change). When the thermal stresses achieve the yield stress, plastic zones can be formed in the matrix near the interfaces, especially, in the vicinity of fibre ends.

With addition of the reinforcing phase, the geometrically necessary dislocations are generated to accommodate the mismatch of plastic deformation in the matrix. The density of the geometrically necessary dislocations may be expressed as [28]:

$$\rho_{\mathrm{G}} = \frac{f8\varepsilon_{\mathrm{p}}}{bt_{\mathrm{m}}}, \tag{11}$$

where ε_{p} is the plastic strain. The influence of the

Table 1. The most important strengthening mechanisms in composites

Mechanism		
Load transfer	$\sigma_{\mathrm{LT}} = \sigma_{\mathrm{m}} \left[1 + \frac{(L + d_{\mathrm{t}})\, A}{4L}\right] f + \sigma_{\mathrm{m}} (1 - f)$	L – fibre length, d_{t} – fibre thickness, $A = (L/d_{\mathrm{t}})$, f – volume fraction, σ_{m} –matrix stress
Thermal dislocations	$\rho_{\mathrm{T}} = \frac{B f \Delta\alpha\, \Delta T}{b(1-f)} \frac{1}{t_{\mathrm{m}}}$	b – Burgers vector, $B = 10$ for fibres and $B = 12$ for particles, $\Delta\alpha\Delta T$ – thermal strain
Dislocation geometrically necessary	$\rho_{\mathrm{G}} = \frac{f 8 \varepsilon_{\mathrm{p}}}{b t_{\mathrm{m}}}$	ε_{p} – plastic strain
Enhanced dislocation density	$\Delta\sigma_{\mathrm{D}} = \alpha_1 \psi G b \left(\rho_{\mathrm{T}} + \rho_{\mathrm{G}}\right)^{1/2}$	α_1 – constant, ψ – Taylor factor, G – shear modulus
Orowan strengthening	$\Delta\sigma_{\mathrm{OR}} = \frac{Gb}{\Lambda} + \frac{5}{2\pi} G f \varepsilon_{\mathrm{p}}$	Λ – distance between fibres
Grain size refinement	$\Delta\sigma_{\mathrm{GS}} = K_{\mathrm{y}} \left(d_2^{-1/2} - d_1^{-1/2}\right)$	K_{y} – constant, d_1, d_2 – grain size
Average residual stress in matrix	$\langle\sigma_{\mathrm{m}}\rangle_{\max} = \frac{2}{3}\sigma_{\mathrm{y}} \ln\left(\frac{1}{f}\right) \frac{f}{1-f}$	σ_{y} – yield stress in matrix

geometrically necessary dislocations increases with increasing strain.

Introducing the reinforcing phases into the metal matrix influences not only the densities of the thermally formed and geometrically necessary dislocations, but also the dislocations stored at reinforcements during deformation. Considering these effects, the total dislocation density in composites can be written:

$$\rho_{\mathrm{total}} = \rho_{\mathrm{T}} + \rho_{\mathrm{G}} + (\rho_{\mathrm{S}} + \rho_{\mathrm{a}}), \tag{12}$$

where ρ_{S} is the statistically stored dislocation density in unreinforced matrix, ρ_{a} is the diminished part of the statistically stored dislocations due to the addition of a reinforcing phase. The strengthening in the matrix is attributed to the deformation resistance induced by the reinforcing phase. According to Taylor relation, the contribution to the total stress due to the presence of dislocations in the matrix may be written:

$$\Delta\sigma_{\mathrm{D}} = \alpha_1 \psi G b \left(\rho_{\mathrm{T}} + \rho_{\mathrm{G}} + \rho_{\mathrm{S}} + \rho_{\mathrm{a}}\right)^{1/2}. \tag{13}$$

This higher matrix dislocation density as well as the reinforcement/matrix interfaces can provide high diffusivity paths in a composite. Such possibility may play an important role in the softening processes.

Among other possible strengthening mechanisms the Orowan strengthening [29], grain refinement and residual thermal stresses may be considered [30]. A brief summary of the strengthening mechanisms in composites is given in Table 1. The models, and also the experimental behaviour, show that a composite strengthening depends on the geometrical parameters of reinforcements (size and shape of fibres or particles, volume fraction of the reinforcement, interparticle distance), on the physical properties of the components (thermal expansion coefficient, binding at the interface matrix-reinforcement), on microstructure and mechanical properties of the components. Individual contributions to the strengthening, calculated using constants introduced in Table 3, are summarised in Table 2. From Table 2 it is obvious that the enhanced dislocation density may significantly increase the composite flow stress. The load transfer is also an important strengthening mechanism in the composites reinforced by short fibres. Other strengthening mechanisms have a marginal importance for the composite strength. Comparing the calculated value of the total stress with the experimental one it follows that the measured value is lower. This may be caused by two reasons:

(i) The models used for calculations are constructed for the perfect binding between the matrix alloy and the Saffil fibres. Such binding depends on the binder used in the perform (in this case starch with the Al_2O_3 powder) and on the chemical reaction between matrix and fibres.

(ii) There is, however, a question how to sum the individual contributions. According to Lilholt [36] the stress contributions, which act more or less uniformly

Table 2. Contributions of various strengthening mechanisms to the yield stress of the composite at room temperature

σ_{02} alloy (MPa)	$\Delta\sigma_{LT}$ (MPa)	$\Delta\rho_T$ (m^{-2})	$\Delta\rho_G$ (m^{-2})	$\Delta\sigma_D$ (MPa)	$\Delta\sigma_{OR}$ (MPa)	$\Delta\sigma_{GS}$ (MPa)	$<\sigma_m>_{max}$ (MPa)	σ_{tot} (MPa)	σ_{exp} (MPa)
68	36	1.78×10^{13}	2.2×10^{12}	51	2	15	13.8	185.8	168.3

Table 3. Constants used for calculation of contributions to the yield stress given in Table 2

α(AX41) (K^{-1})	α(Saffil) (K^{-1})	G (GPa)	K_y (MPa $m^{-3/2}$)	b (m)	Taylor factor ψ	α_1
25×10^{-6} [31]	6×10^{-6} [32]	17	0.28 [33]	3.2×10^{-10}	6 [34]	0.35 [35]

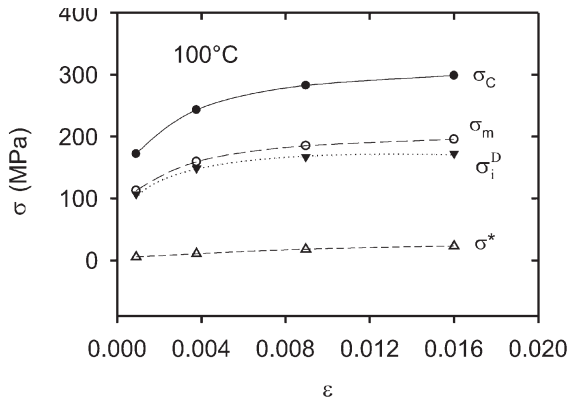

Fig. 6. A part of the true stress-true strain curve at 100 °C. Points indicate the stresses at which the SR tests were performed.

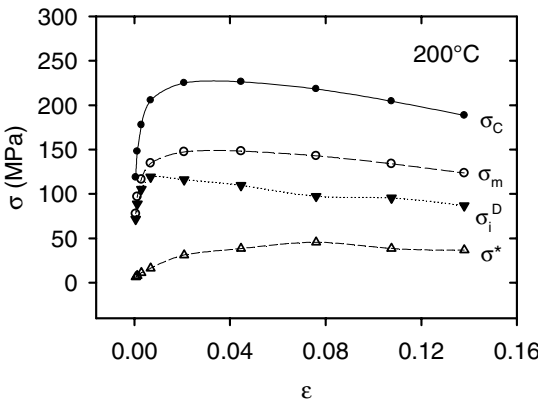

Fig. 7. A part of the true stress-true strain curve at 200 °C. Points indicate the stresses at which the SR tests were performed.

throughout the matrix, must be superimposed linearly, whereas mechanisms of similar strengthening ability, which act unevenly throughout the matrix, are most suitably combined as the square root of the sum of the squares [37]. For the yield stress of the composite at room temperature, one obtains 185.8 MPa using the linear superposition in comparison to 134 MPa for a quadratic sum.

4.2. Internal stress in the matrix

The stress components (σ_i^D, σ^*) were estimated from the stress relaxation curves. A part of the stress--strain curve for specimens deformed at 100 °C is shown in Fig. 6. Full circles depict points at the stress--strain curve where the stress relaxation tests were performed. Blank circles indicate the matrix stress and full and blank triangles designate the internal stress σ_i^D and the effective stress σ^*, respectively. It is obvious that the internal stress σ_i^D is a substantial contribution to the matrix stress σ_m. A similar analysis was performed at 200 °C and introduced in Fig. 7. As it follows from Fig. 7 the internal stress increases with strain only in the very beginning of deformation; for strains higher than about 2 %, it decreases with strain while the effective stress increases continuously up to a true strain of 8 %. For higher strains, the effective stress remains constant, while the applied stress is decreasing. Comparison of the internal stress estimated for the AX41 alloy and that for the composite with the AX41 matrix reinforced with the 13 % of Saffil fibres is introduced in Fig. 8. Subtracting the value of the load transfer $\Delta\sigma_{LT}$, it can be seen that the internal stress level in the composite is higher in comparison with the unreinforced alloy. The difference exhibiting 64.5 MPa is due to a higher dislocation density of thermal dislocations ($\rho_T = 1.78 \times 10^{13}$ m^{-2}) and dislocations geometrically necessary ($\rho_G = 1.4 \times 10^{13}$ m^{-2}). Corresponding stress $\Delta\sigma_\rho = \alpha\psi Gb(\Delta\rho)^{1/2} =$ 64.4 MPa.

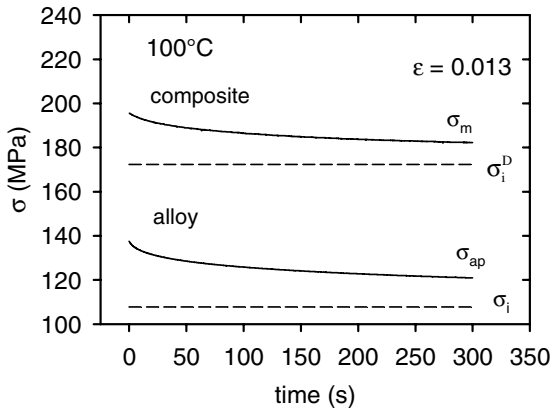

Fig. 8. Comparison of the dislocation internal stress estimated at 100 °C and at a strain of 0.013 for the composite and the monolithic alloy.

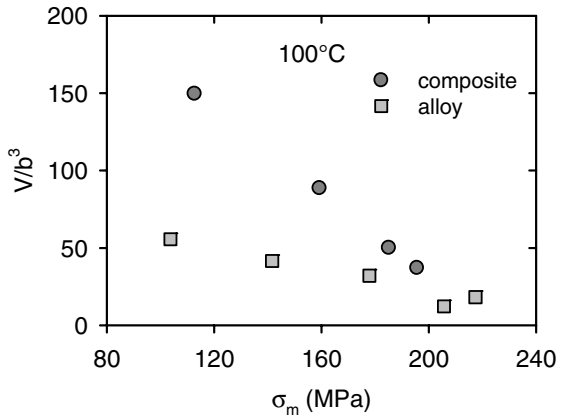

Fig. 9. Activation volume in b^3 depending on the stress in the matrix estimated for the composite and the monolithic alloy.

4.3. Thermal activation

The values of the activation volume V_{app} were estimated according (8) and (9) using stress decrease in the matrix ($\sigma_{\mathrm{m}} = \sigma_{\mathrm{app}} - \Delta\sigma_{\mathrm{LT}}$). As usual, the values of the activation volume are divided by b^3. The values for samples deformed at 100 °C are plotted against the matrix stress σ_{m} in Fig. 9. For comparison, the values of the activation volume (divided by b^3) estimated for unreinforced alloy at temperature of 100 °C are also introduced. If the same values of the activation volume are plotted against the effective stress σ^*, all data lie on one line – "master curve" (Fig. 10). Kocks et al. [38] suggested an empirical equation between the Gibbs enthalpy ΔG and the effective stress σ^* in the following form:

$$\Delta G = \Delta G_0 \left[1 - \left(\frac{\sigma^*}{\sigma_0^*}\right)^p\right]^q, \qquad (14)$$

where ΔG_0 and σ_0^* are Gibbs enthalpy and the effective stress at 0 K. For the effective stress it follows:

$$\sigma^* = \sigma_0^* \left[1 - \left(\frac{kT}{\Delta G_0} \ln \frac{\dot{\varepsilon}_0}{\dot{\varepsilon}}\right)^{1/q}\right]^{1/p}, \qquad (15)$$

where p and q are phenomenological parameters reflecting the shape of a resistance obstacle profile. The possible ranges of values p and q are limited by the conditions $0 < p \leq 1$ and $1 \leq q \leq 2$. Ono [39] suggested that Eq. (14) with $p = 1/2$, $q = 3/2$ describes a barrier shape profile that fits many predicted barrier shapes. Thermodynamics generally defines the activation volume as:

$$V = -\left(\frac{\mathrm{d}\Delta G}{\mathrm{d}\sigma^*}\right)_{\mathrm{T}} = kT\left(\frac{\mathrm{d}\ln\dot{\varepsilon}}{\mathrm{d}\sigma^*}\right)_{\mathrm{T}} = kT\left(\frac{\mathrm{d}\ln(-\dot{\sigma})}{\mathrm{d}\sigma^*}\right)_{\mathrm{T}}. \qquad (16)$$

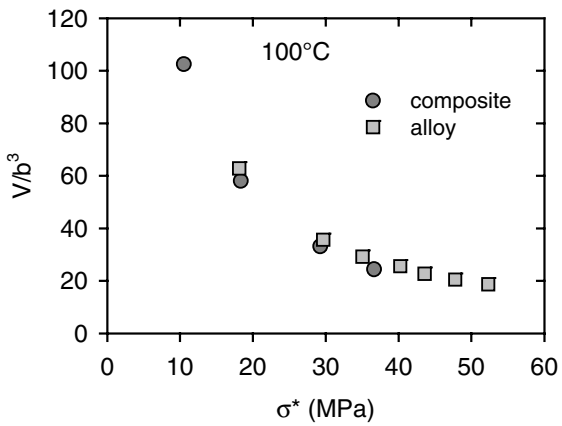

Fig. 10. The plot of the activation volume in b^3 against the effective stress estimated at 100 °C for the composite and the monolithic alloy.

Equation (16) can be rewritten as:

$$V = \frac{\Delta G_0 pq}{\sigma_0^*}\left[1 - \left(\frac{\sigma^*}{\sigma_0^*}\right)^p\right]^{q-1}\left(\frac{\sigma^*}{\sigma_0^*}\right)^{p-1}. \qquad (17)$$

The values of the activation volume lie at the curve given by Eq. (16), as it is obvious from Fig. 11.

The activation enthalpy $\Delta H = \Delta G - T\Delta S$ (ΔS is the entropy) is done by

$$\Delta H = -TV\frac{\mathrm{d}\sigma}{\mathrm{d}T}. \qquad (18)$$

The differential coefficient $\mathrm{d}\sigma/\mathrm{d}T$ was estimated to be 0.159 MPa K^{-1} from the temperature dependence of the yield stress in the temperature range from 100 to 200 °C. The activation enthalpy calculated according to (17) for 200 °C gives (0.95 ± 0.05) eV. Similar

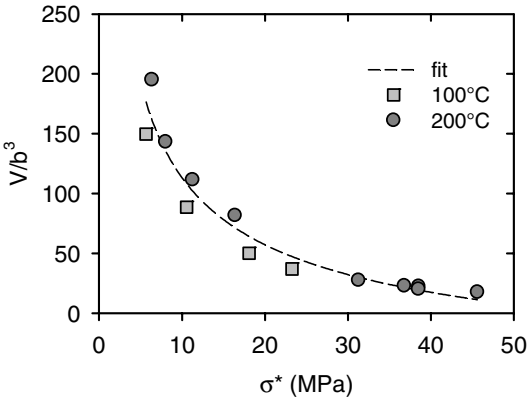

Fig. 11. The plot of the activation volume in b^3 against the effective stress estimated at two temperatures for the composite.

value of 0.96 eV has been reported for AX41 alloy [40] and Mg in creep experiments at 400 K [41]. A rapid decrease of the flow stress at elevated temperatures indicates the possible occurrence of recovery process(-es) that is usually thermally activated. The values of the activation volume and the activation enthalpy may help to identify this thermally activated process. The thermally activated processes occurring in the AX41 alloy during plastic deformation at temperatures higher than ambient temperature have been studied using stress relaxation tests in our previous paper [40]. The activation of the prismatic slip and subsequent annihilation of the dislocation segments with the opposite sign have been found as the main reason for the observed internal stress decrease. The double cross slip and the thermally activated glide of the $\langle c+a \rangle$ dislocations in pyramidal planes should be taken into account. Because the values of the activation volume and activation energy are very similar to those estimated for monolithic AX41 alloy, we can conclude that the thermally activated processes are the same.

5. Conclusions

The main results of the complex analysis of the deformation mechanisms in the AX41 alloy reinforced with 13 vol.% of short Saffil fibres:

– the main contribution to the composite strengthening originates from the increased dislocation density;

– the load transfer from the matrix to the reinforcing phase fibres is also important contribution;

– the internal stress estimated from the stress relaxation tests decreases with increasing deformation temperature;

– the values of the apparent activation volumes are in the order of 10^1–10^2 b^3;

– estimated values of the activation energy are the same as estimated for the monolithic alloy;

– the estimated parameters of the thermally activated deformation showed that the main thermally activated process is very probably the glide of dislocations in the non-compact planes.

Acknowledgements

The authors thank the Grant Agency of the Czech Republic for financial support under grant 106/06/1354. A part of this work was financed by the Ministry of Education of the Czech Republic under the research project MSM 0021620834.

References

[1] LEYENS, C.—PETERS, M.: Titanium and Titanium Alloys – Fundamentals and Applications. Weinheim, Wiley-VCH 2005.
[2] TROJANOVÁ, Z.: Kovove Mater., *43*, 2005, p. 182.
[3] RUDAJEVOVÁ, A.—MUSIL, O.: Kovove Mater., *43*, 2005, p. 210.
[4] JANEČEK, M.—ŠUPÍK, V.—HOLLÄNDER, F.—WENDT, J.: Kovove Mater., *43*, 2005, p. 218.
[5] MÁTHIS, K.—TROJANOVÁ, Z.: Kovove Mater., *43*, 2005, p. 238.
[6] NOVÝ, F.—PALČEK, P.—CHALUPOVÁ, M.: Kovove Mater., *43*, 2005, p. 447.
[7] TROJANOVÁ, Z.—LUKÁČ, P.: Kovove Mater., *43*, 2005, p. 73.
[8] HNILICA, F.—OČENÁŠEK, V.—STULÍKOVÁ, I.—SMOLA, B.: Kovove Mater., *43*, 2005, p. 300.
[9] TROJANOVÁ, Z.—MILNERA, M.: Kovove Mater., *44*, 2006, p. 75.
[10] ORLOVÁ, A.—KUCHAŘOVÁ, K.—DLOUHÝ, A.: Kovove Mater., *43*, 2005, p. 55.
[11] LAPIN, J.: Kovove Mater., *43*, 2005, p. 81.
[12] LAPIN, J.: Kovove Mater., *44*, 2006, p. 57.
[13] LAPIN, J.: Intermetallics, *14*, 2006, p. 115.
[14] PAHUTOVÁ, M.—SKLENIČKA, V.—KUCHAŘOVÁ, K.—SVOBODA, M.—LANGDON, T. G.: Kovove Mater., *43*, 2005, p. 34.
[15] MILIČKA, K.—DOBEŠ, F.: Kovove Mater., *43*, 2005, p. 45.
[16] LUKÁČ, P.—TROJANOVÁ, Z.: Kovove Mater., *44*, 2006, p. 243.
[17] TROJANOVÁ, Z.—RUDAJEVOVÁ, A.—PADALKA, O.—JANEČEK, M.—LUKÁČ, P.: Kovove Mater., *44*, 2006, p. 283.
[18] DOBEŠ, F.—MILIČKA, K.: Kovove Mater., *43*, 2005, p. 66.
[19] BESTERCI, M.—VELGOSOVÁ, O.: Kovove Mater., *43*, 2005, p. 229.
[20] TJONG, S. C.: Adv. Eng. Mater., *9*, 2007, p. 639.
[21] AIKIN, Jr., R. M.—CHRISTODOULU, L.: Scripta Metall. Mater., *25*, 1991, p. 9.
[22] DOTSENTKO, V. I.: Phys. Stat. Sol. (b), *93*, 1979, p. 11.
[23] FELTHAM, P.: Phys. Stat. Sol., *3*, 1963, p. 1340.

[24] LI, J. C. M.: Canad. J. App. Phys., *45*, 1967, p. 493.
[25] DE BATIST, R.—CALLENS, A.: Phys. Stat. Sol. (a), *21*, 1974, p. 591.
[26] TROJANOVÁ, Z.—DROZD, Z.—KÚDELA, S.—SZÁRAZ, Z.—LUKÁČ, P.: Comp. Sci. Techn., *67*, 2007, p. 1965.
[27] ARSENAULT, R. J.—SHI, N.: Mater. Sci. Eng., *81*, 1986, p. 151.
[28] ASHBY, M. F.: Phil. Mag., *21*, 1970, p. 399.
[29] SCATTERGOOD, R. O.—BACON, D.: Phil. Mag. A, *31*, 1975, p. 179.
[30] DELANNAY, F.: In: Comprehensive Composite Materials. Vol. 3. Ed.: Clyne, T. W. Amsterdam, Elsevier 2000, p. 341.
[31] TROJANOVÁ, Z.—PADALKA, O.—LUKÁČ, P.—SZÁRAZ, Z.: (to be published).
[32] Handbook of Chemistry and Physics. 73rd edition. Ed.: Lide, D. R. Boca Raton, USA, CRC Press 1992–1993.
[33] MABUCHI, M.—HIGASHI, K.: Acta Mater., *44*, 1996, p. 4611.
[34] ARMSTRONG, R. W.: Acta Metall., *16*, 1968, p. 347.
[35] LAVRENTEV, F. F.—POKHIL, Y. A.—ZOLUTKHINA, I. N.: Mater. Sci. Eng., *32*, 1978, p. 113.
[36] LILHOLT, H.: Mater. Sci. Eng. A, *135*, 1991, p. 161.
[37] CLYNE, T.—WHITHERS, P. J.: An Introduction to Metal Matrix Composites. Cambridge, Cambridge Press 1993.
[38] KOCKS, U. F.—ARGON, A. S.—ASHBY, M. F.: Progr. Mater. Sci., *19*, 1975, p. 1.
[39] ONO, K.: J. Appl. Phys., *39*, 1968, p. 1803.
[40] TROJANOVÁ, Z.—LUKÁČ, P.—KAINER, K. U.: Adv. Eng. Mater., *9*, 2007, p. 370.
[41] MILIČKA, K.—ČADEK, J.—RYŠ, P.: Acta Metall., *18*, 1970, p. 1071.